



# Electrochemical Response of Redox Amino Acid Encoded Fluorescence Protein for Hydroxychloroquine Sensing

Asuma Janeena<sup>1,2</sup> · Narayanan Jayaraman<sup>3</sup> · Ganesh Shanmugam<sup>2,4</sup> · Shanmugam Easwaramoorthi<sup>2,3</sup> · Niraikulam Ayyadurai<sup>1,2</sup>

Accepted: 28 August 2022 / Published online: 19 October 2022

© The Author(s), under exclusive licence to Springer Science+Business Media, LLC, part of Springer Nature 2022

## Abstract

The sudden rise in the demand has led to large-scale production of hydroxychloroquine (HCQ) in the global market for various diseases such as malaria, rheumatic arthritis, and systemic lupus erythematosus and prophylactic treatment of early SARS-CoV-2 outbreak. Thorough monitoring of HCQ intake patients is in high demand; hence, we have developed a redox amino acid encoded fluorescent protein-based electrochemical biosensor for sensitive and selective detection of HCQ. This electrochemical biosensor is generated based on the two-electron transfer process between redox amino acid (3,4-dihydroxy-L-phenylalanine, DOPA) encoded bio-redox protein and the HCQ forms the conjugate. The DOPA residue in the bio-redox protein specifically binds with HCQ, thereby producing a remarkable electrochemical response on the glassy carbon electrode. Experimental results show that the developed biosensor selectively and sensitively detects the HCQ in spiked urine samples. The reagent-free bio-redox capacitor detects HCQ in the range of 90 nM to 4.4 μM in a solution with a detection limit of 58 nM, signal to noise ratio of 3:1, and strong anti-interference ability. Real-time screening, quantification, and relative mean recoveries of HCQ on spiked urine samples were monitored through electron shuttling using bio-redox protein and were found to be 97 to 101%. Overall, the developed bio-redox protein-based sensor has specificity, selectivity, reproducibility, and sensitivity making it potentially attractive for the sensing of HCQ and also applicable to clinical research.

**Keywords** Chitosan · Hydroxychloroquine · Bio-redox protein · Biosensor · L-3,4-dihydroxyphenylalanine · Electron transfer

---

Asuma Janeena and Narayanan Jayaraman contributed equally to this work.

✉ Shanmugam Easwaramoorthi  
moorthi@clri.res.in

✉ Niraikulam Ayyadurai  
ayyadurai@clri.res.in

Extended author information available on the last page of the article

## Introduction

Hydroxychloroquine (HCQ) is amino-4-quinoline, a derivative of quinolone, and is majorly used as a therapeutic drug for a wide range of diseases such as malaria, rheumatoid arthritis, and systemic lupus erythematosus [1–5]. HCQ is metabolized into desethylchloroquine, bis-desethylchloroquine, and monodesethylchloroquine. Among them, monodesethylchloroquine is the most active metabolite and is involved in four major activities. HCQ increases the intracellular pH, resulting in decreased phagolysosome fusion and impeding viral receptor glycosylation. It inhibits the endosomal Toll-like receptors (TLRs) 7 and 9 which results in the inactivation of cytokine signaling pathways. Activation of NADPH oxidase is restricted by HCQ thereby increasing the reactive oxygen species (ROS) resulting in the signaling cascade of TNF and IL-1. Finally, HCQ blocks the calcium transport from the endoplasmic reticulum leading to the impairment of signaling pathways which is needed for cytokine expression and secretion. Due to its pleomorphic effects, HCQ was administered for the early SARS-CoV-2 outbreak, and due to various side effects, the same has been withdrawn from usage [6–13].

Pharmacologically, HCQ has a notably extended half-life (20 to 60 days) and reaches peak plasma concentration within 3 to 4 h, and in urine, HCQ could be detected for up to 90 days [14, 15]. For patients, HCQ in combination with other drugs has been recommended, but prolonged use of HCQ results in a life-threatening cardiac arrest, retinopathy, kidney, nerve cell damage, etc. Hence, it is inevitable to develop therapeutic drug monitoring (TDM) of HCQ to prescribe suitable administrative dose levels [16–18]. The reliability of drug monitoring is related to the specificity and sensitivity of the method used to quantify drugs in fluids. Chromatography, immunoassay, and mass spectrometry approaches are well known among them. Nevertheless, these methods are restricted by their turn-around times, difficulty in handling a large number of samples, high instrumentation cost, and strenuous sample preparation [19]. In the present scenario, it is of paramount importance to develop a simple, selective, sensitive TDM tool for HCQ sensing, with unique features to overcome these limitations.

Integrating biological components into microfabricated devices could serve as an ideal biosensor. It will allow monitoring of the signal changes via electrochemical devices and allows the creation of a sensitive biosensor for the detection and quantification of drug molecules [20]. Biological networks are naturally encoded with a diverse form of redox communication, but most of the metabolic signals are electrochemically distant without additional engineering [21]. For an effective bio-electronic interface, it is important to develop direct electronic integration of redox communication networks to interact with the biological system [22–28]. A potent method to enhance electrons and protons for signal processing was through homogenous grafting of the biopolymer on the electrode. Chitosan is an amino-polysaccharide, highly biocompatible, and can easily shuttle electrons to the electrode. Frequently, chitosan-fabricated electrodes were grafted with reactive ortho-quinone intermediate from catechol through Schiff base or Michael-type adduct formation. Catechols are well known for diverse biological functions; especially they yield reactive redox-based quinone intermediate for the non-enzymatic reaction [29, 30]. Recently, we have genetically introduced the signal responsive catecholic non-canonical amino acid L-3,4-dihydroxyphenylalanine (DOPA) in green fluorescent protein (GFP). The designer protein encoded with catechol (DOPA) is well known for its adhesive chemistry through metal bidentate coordination and hydrogen bonding. On the other hand, DOPA is a redox-active amino acid and its oxidation will lead to the form of o-quinone comprising

the reactive nucleophilic group. The redox DOPA could switch between oxidized (Q) and reduced (QH<sub>2</sub>) states by exchanging electrons with diffusible mediators in a thermodynamically constrained process to establish a signal to sense HCQ. Therefore, we biosynthesized the redox-active amino acid encoded (DOPA) protein through genetic code engineering and it exhibits highly stable and easily fabricated on the electrode surface. Hence, electrode coating with catecholic amino acid encoded proteins would have better selectivity, tunable functional properties, ease in fabrication, and enzymatically removable without damaging the fabricated structure. Here, the genetically encoded bio-redox capacitor will act as an electron acceptor and the drug act as an electron donor and this charge transfer process could be monitored in real-time. The bio-redox protein (GFP DOPA) was electrochemically fabricated with chitosan and genetically encoded GFP DOPA (chitosan-GD) for selective and sensitive detection of minimum HCQ drug levels, in patient epitome samples.

## Experimental Section

### Reagents and Materials

The expression host *Escherichia coli* (*E. coli*) tyrosine auxotroph was received from Coli Genetic Stock Center, and the pQE80-L vector was purchased from Qiagen (Valencia, USA). T4 DNA ligase and restriction enzymes were purchased from New England Biolabs (Ipswich, US). Natural amino acids, M9 salts, 3,4-dihydroxy-L-phenylalanine (L-Dopa), ferrocene carboxaldehyde 98%, and chitosan (medium molecular weight) were purchased from Sigma-Aldrich (Bangalore, India). Isopropyl β-d-1-thiogalactopyranoside (IPTG), ampicillin, Luria–Bertani (LB) broth, and imidazole were purchased from HiMedia (Mumbai, India). His trap HP protein purification column was purchased from GE Healthcare (Bangalore, India). Used as a working buffer solution was 0.01 M phosphate buffer saline pH 7.4. Chitosan solutions (2%, pH 5.5) were prepared by dissolving chitosan in 0.25 N HCl.

### Construction of Plasmids, Strains, and Incorporation of Unnatural Amino Acids

The DNA manipulations were performed as described earlier [31]. The plasmid pQE60-L bearing GFP gene was amplified by gene-specific primers and cloned into pQE80-L using restriction enzymes (Bam HI and Hind III), which resulted in pQE80-GFP. The construct of pQE80-GFP was transformed into *E. coli* JW2581 tyrosine auxotroph for the non-canonical amino acid (NCAA) incorporation as described earlier [32].

### Protein Expression and Purification

The successfully cloned pQE80-GFP was grown in LB broth [33]. After attaining the mid-log phase (0.6 OD 600), the cells were induced with 1 mM isopropyl β-D-1-thiogalactopyranoside (IPTG) and incubated at 37 °C for 6 h. Simultaneously, the GFP-DOPA (GD) expression was also carried out in the same *E. coli* auxotrophic cells bearing pQE80-GFP. The cells were grown in the minimal medium depleted with 0.3 mM tyrosine until it reaches the mid-log phase (0.8–1 OD). Later, the tyrosine analog, L-Dopa (1 mM), was added and induced with 1 mM IPTG. After expression, the cells were ruptured in a

high-pressure homogenizer (Stansted, Essex, UK) and the proteins were purified using a His-trap HP column. Furthermore, the purified protein (GFP Dopa, GD) was subjected to the gel permeation chromatography by AKTA Explorer FPLC system containing Superdex G25 HR column at 25 °C.

### Interaction of HCQ with GD Using Spectroscopic Studies

The purified protein GFP DOPA (4  $\mu\text{M}$ ) was subjected to a spectrofluorometer in the presence and absence of HCQ at various concentrations, 0–210  $\mu\text{M}$  in 10 mM phosphate buffer pH 7.4 (JASCO FP-777, Tokyo, Japan). The fluorescence spectra acquired excitation,  $\lambda_{\text{ex}} = 470$  nm, and emission,  $\lambda_{\text{em}} = 480\text{--}600$  nm, at 298 K. The interference of other quinone-based drugs (210  $\mu\text{M}$  concentration of mefloquine, primaquine, chloroquine, and HCQ) with GD was also subjected to fluorescence spectrometer. To understand the interaction of HCQ with GD, various concentrations of HCQ with GD were subjected and analyzed using CD spectrometer. The obtained molar ellipticity spectra was converted to mean residue ellipticity by dividing with the number of amino acid residues in the protein. The resulting spectra were used for percentage calculation with the help of CD pro software.

### Interaction of HCQ with GD by STD NMR

The NMR experiments were carried out at 293 K on an ECA-500 JEOL spectrometer operating at 500 MHz (11.74 T). The STD NMR requires the ligand concentration at least 100-fold higher than protein. Hence, the ligand and protein concentrations were maintained at 50 mM and 5  $\mu\text{M}$ , and the respective ligand to protein ratios of 100:1 for HCQ and GD. As reported by Mayer et al. (2001) in the present studies, STD pulse sequence additionally involves water suppression. Selective presaturation of the protein was done with the help of Gaussian-shaped pulses of 60-ms length and separation delayed by 1 ms. The number of selective pulses ( $n$ ) of the saturation period was 40 followed by a saturation total length of 2.4 s. The on- and off-resonance irradiation of protein were done at a chemical shift of 0.5 ppm and 30 ppm where ligand signals were absent. The exponential line broadening of 3 Hz was applied to the FID corresponding to the difference in the off- and on-resonance position and Fourier transformed. Five-seconds relaxation delay was used in the STD measurements for long relaxation time to the ligands. 1 D STD NMR and STD profiles were measured with 7400 scans using an inverse probe, and a 50-ms T1p filter was used to remove the protein background signals.

### Electrochemical Set-Up and Apparatus

All the electrochemical experiments were carried out using CHI660E CH instruments, and the experiments were performed by using three-electrode systems consisting of a platinum wire as a counter electrode, Ag/AgCl as a reference electrode, and glassy carbon electrode (GCE 3 mm), chitosan/GCE (chitosan), and GFP DOPA/chitosan/GCE electrodes (chitosan-GD) as a working electrode. The differential pulse voltammetry (DPV) measurements were carried out in 0.01 M phosphate buffer saline pH 7.4. Electrochemical impedance spectroscopy (EIS) study was carried out in 5 mM  $\text{Fe}(\text{CN})_6^{3-/4-}$  containing 0.01 M phosphate buffer saline pH 7.4 with a frequency range from 0.1 Hz to 100 kHz at a potential 0.2 V.

## Fabrication of Bio-redox Capacitor

We dissolved 1.6 gm of chitosan flakes in 100 ml of cold 0.25 N HCl solution with vigorous stirring and kept at 4 °C for overnight [34]. The pH of the dissolved chitosan solution was adjusted to 5.8–6.8 by adding 1 M NaOH. Furthermore, this solution was used for electrode fabrication.

The steps involved in bio-redox protein anodic electrodeposition of chitosan film fabrication are illustrated in Scheme 1. The GCE was polished with 0.3 μm alumina slurry on a micro cloth pad and washed with DI water. The GCE electrode was modified with a chitosan film via an anodic electrodeposition reaction. The GCE surface was modified with chitosan solution (2%) by applying an anodic current of 0.25 A for 800 s. After, the chitosan film-modified electrode was immersed in 4 μM of bio-redox protein in N<sub>2</sub> saturated 0.01 M PBS solution for electro grafting by applying a constant potential of +0.6 V (vs Ag/AgCl) for 400 s. After fabrication, the electrode was air-dried and stored at 4 °C for further analysis.

## Surface Morphological Characterization of Electrode

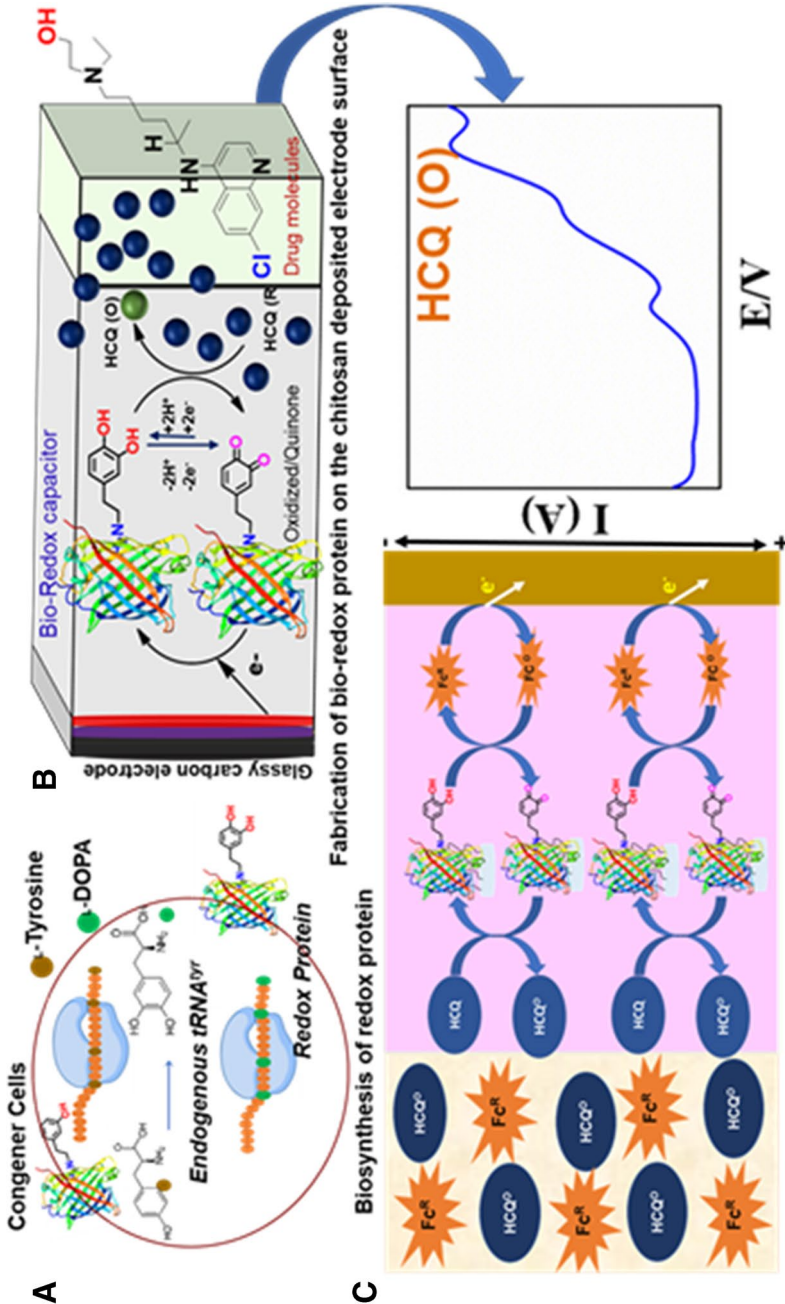
The electrodes were modified with chitosan and dried. Later, the modified chitosan electrode was further deposited with GD. The surface morphological characterization of electrodes was carried out by field emission scanning electron microscopy (FE-SEM, CLARA, TESCAN, Czech) at an operating voltage of 500 eV. Atomic force microscopic (AFM) images were recorded by NTEGRA PRIMA, NT-MDT, Russia. The chitosan films and GD electrografted chitosan films were chemically analyzed using X-ray photoelectron spectroscopy (XPS, Omicron ESCA Probe spectrometer with unmonochromatized Mg KR X-rays (energy) 1253.6 eV, 300 W). All the spectra were deconvoluted to their component peaks, using the software CASA-XPS.

## Differential Pulse Voltammetry Analysis

The fabricated electrode containing bio-redox protein impregnated chitosan matrix was rinsed with DI water, and differential pulse voltammetry (DPV) was carried out by applying potential from –0.2 to 1.2 V at a scan rate of 10 mV/s in a 0.01 M PBS pH 7.4 solution containing 5 μM ferrocene and different concentration of hydroxychloroquine (HCQ).

## Detection of HCQ in Spiked Urine Samples

The performance and reliability of the developed genetically encoded bio-redox protein towards HCQ sensing were assessed in real urine samples and were spiked with various concentrations of HCQ and diluted to 10 ml with 0.01 mM PBS at pH 7.4. To perform the standard addition method for the detection of HCQ, the specified amounts of HCQ were spiked into the urine samples before dilution. The samples were kept in a shaker for 30 min and were centrifuged at 15,000 rpm for 10 min, and 0.1 N of NaOH was used for pH neutralization. The supernatant was collected and was carried out for DPV analysis.



**Scheme 1** Redox mechanism of genetically encoded bio-redox protein for the selective and sensitive monitoring of HCQ. **A** In vivo residue-specific incorporation of DOPA in recombinant GFP. **B** Schematic representation of bio-redox protein-modified electrode and the possible redox reactions at the electrode surface. **C** Electron transfer mechanism involving ferrocene; ferrocene acts as an electron shuttle between the fabricated matrix and the electrode from which they can be either electrochemically oxidized or reduced, diffuse into the matrix and diffuse back to electrode to undergo electrochemical reactions to generate electrochemical response

## Results and Discussion

### Biophysical Characterization of Genetically Incorporated Bio-redox Protein

A genetically encoded redox circuit was prepared through residue-specific incorporation of L-3,4-dihydroxyphenylalanine (DOPA), in green fluorescent protein (GFP) as described earlier [35–38]. The migration in SDS-PAGE gel, redox staining, and shift in the mass (MALDI-TOF) of GD confirmed the genetic incorporation of DOPA into GFP (GFP DOPA, GD). The circular dichroism (CD) spectrum of GD showed a negative peak at 216 nm, and this confirms the unique  $\beta$ -can structure conformation.

### Surface and Elemental Characterization of Bio-redox Capacitor Film on the Electrode

The schematic representation of the fabrication of the glassy carbon electrodes of the developed bio-redox protein-based sensor is illustrated in Scheme 1. A monolayer of chitosan was deposited on the glassy carbon electrode by applying an anodic current of 0.25 A for 800 s followed by air drying it for 10 min. Later, a controlled electrochemical deposition of bio-redox protein at 0.6 V current for 400 s was carried out to enhance the sensitivity and capability of the developed bio-redox protein/chitosan/GCE electrode. The surface morphologies of the glassy carbon electrode (GCE), GCE/chitosan (chitosan), and GCE/chitosan/GD (chitosan-GD) were characterized using a field emission scanning electron microscope (FESEM) which confirms that bio-redox capacitor was grafted on the modified electrode surface (Fig. 1A). After chitosan modification, the surface roughness of the electrode has been increased. Further, the redox amino acid encoded protein was fabricated on the chitosan-modified electrode which leads to a decrease in surface roughness and increases in thickness and electrochemically active surface area.

The surface characteristics of the modified surface were gleaned from the X-ray photoelectron spectra (Fig. 1B). The XPS spectra of O 1s were observed at 529.9 eV for chitosan corresponding to C-O. After fabrication of redox protein on the modified chitosan electrode (chitosan-GD), the peak at 529.9 eV is shifted to 531.8 eV and is attributed to N-C=O in Fig. 1B (i). The carbon spectra in the C 1s region corresponds to C-H/C-C and C-NH<sub>2</sub> at 283.5 and 287.6 eV for chitosan film. Similarly, the carbon spectra for redox bio-capacitor modification possess 285 and 288.3 eV corresponding to C-N and N-C=O (Fig. 1B (ii)). The redox-activated bio-capacitor consistently increases the N-C=O peak after the deposition of GD. Similarly, the nitrogen spectra for the N 1s region belong to NHCO-R at 400.2 eV and NH<sub>2</sub> at 399 eV for redox bio-capacitor film and chitosan film (Fig. 1B (iii)). The atomic force microscopy (AFM) image topography supports chitosan was deposited as a thin film (anodic electrodeposition of amino polysaccharide chitosan) on the GCE surface and the Z-scale height is ~600 nm (Fig. 2). After the electro-grafting of GD on this deposited film, the topography of the electrode has been altered along with increased Z-scale height to ~1000 nm, confirming the grafting of GD on the chitosan film. The observed XPS spectral differences gave direct evidence for electro-grafting of GD on chitosan film and were also supported by the FESEM and AFM results.

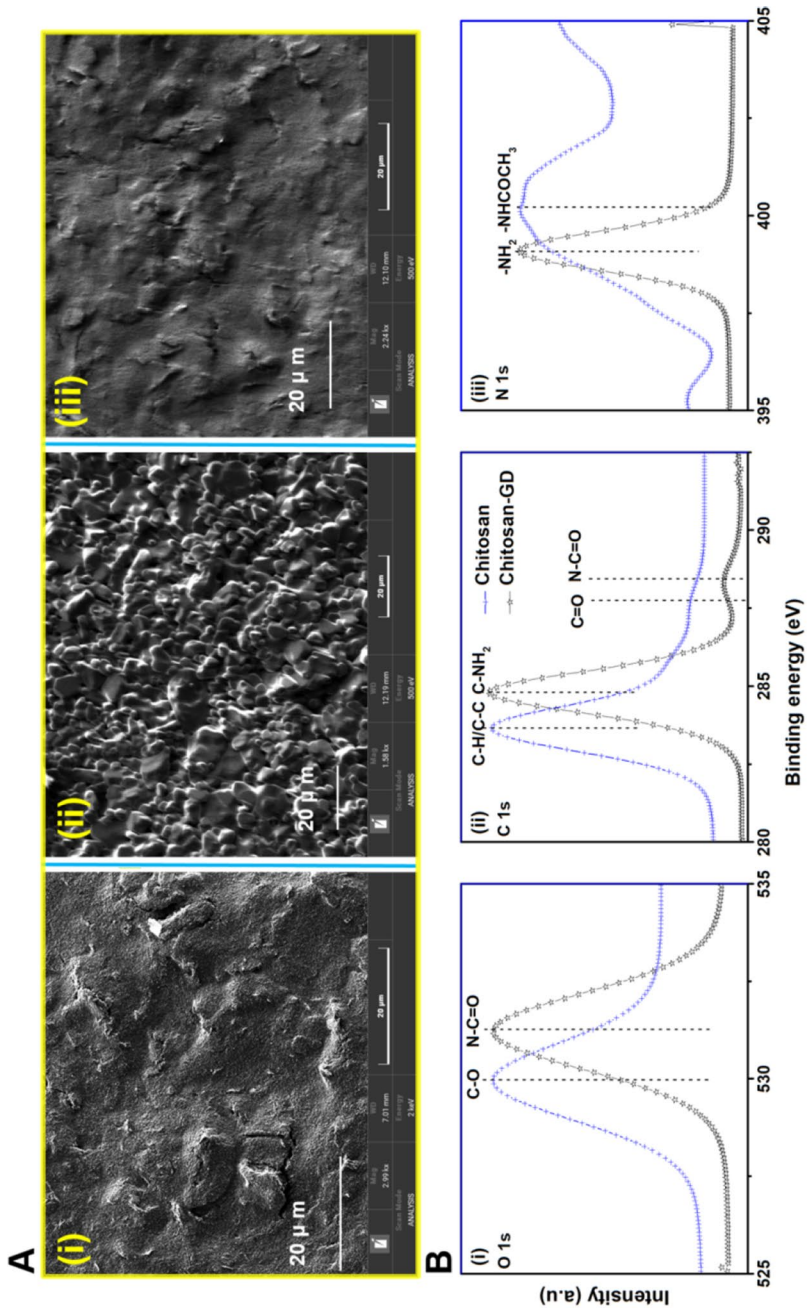


**Fig. 1** A Field emission scanning electron microscope (FESEM) surface morphology images of (i) GCE, (ii) chitosan, and (iii) chitosan-GD. **B** XPS spectra of modified GCE electrode: (i) oxygen spectra, (ii) carbon spectra, and (iii) nitrogen spectra of chitosan and chitosan-GD



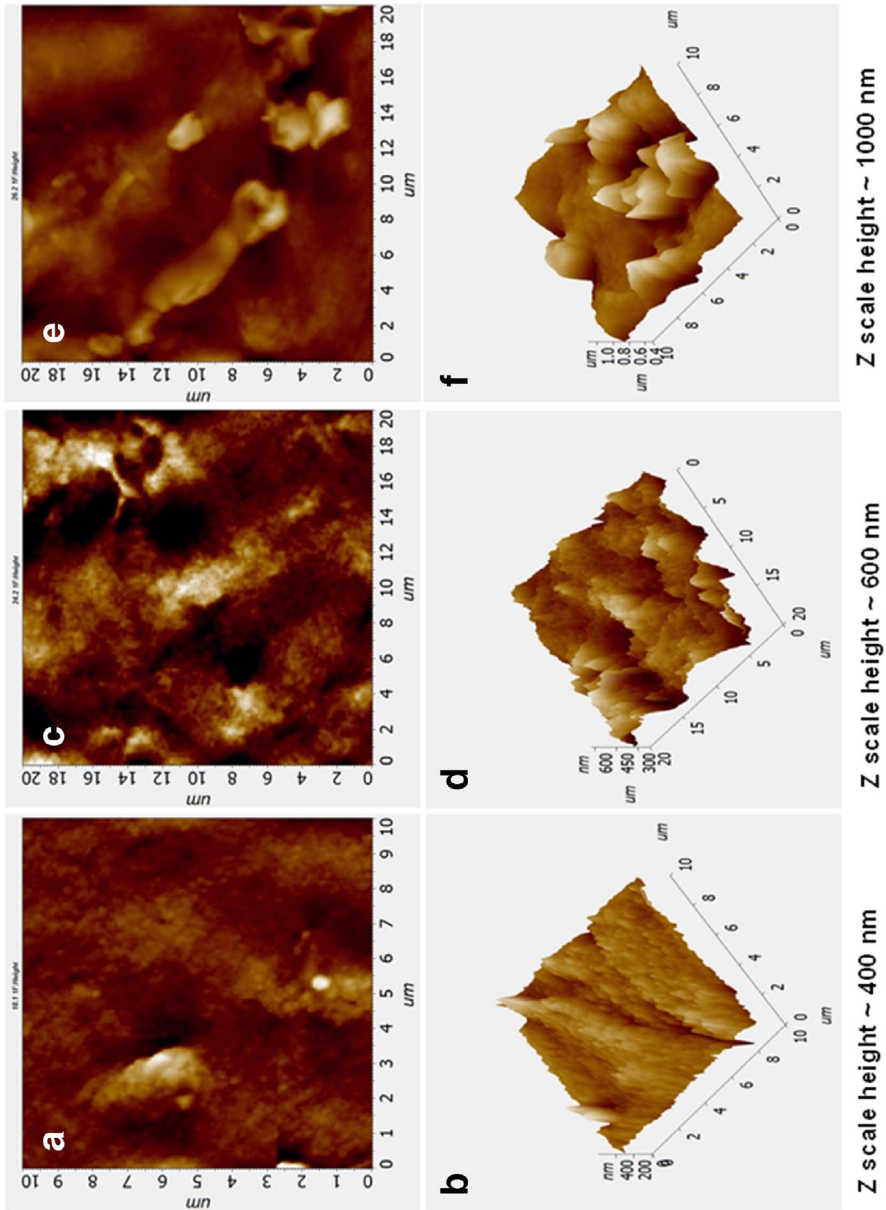


**Fig. 2** Atomic force microscopy (AFM) images of **a** GCE, **b** chitosan/GCE, and **c** GD/chitosan/GCE and their respective 3D image with scale height (image b, image d, and image f)

### Electrochemical Evaluation of Bio-redox Capacitor Film on GCE

Furthermore, the modified GCE was characterized by a differential pulse voltammogram (DPV) to analyze the efficiency to detect the HCQ. The DPVs of bare GCE, chitosan-modified GCE, and chitosan-GD-modified electrodes were recorded in the presence of 1  $\mu\text{M}$  HCQ and 5  $\mu\text{M}$  ferrocene (Fc) in 0.01 M PBS (pH 7.4) at a scan rate of 10 mV/s (Fig. 3A). An oxidation peak at 0.97 V ( $E_{pa}$ ) with 5.8  $\mu\text{A}$  current was observed on the bare GCE electrode (Fig. 3A curve a). After modification with chitosan on GCE, the oxidation current was decreased to 2.5  $\mu\text{A}$  at a peak potential ( $E_{pa}$ ) of 0.99 V which suggests that it hinders the electron transfer on the GCE for the diffusion of electrons from HCQ towards the electrode surface (Fig. 3A curve b). After the electrodeposition of bio-redox protein on the chitosan-modified electrode, the peak current was increased to 7.8  $\mu\text{A}$  at a peak potential ( $E_{pa}$ ) of 1.08 V which indicates better redox behavior of HCQ on the bio-redox protein-modified electrode (Fig. 3A curve c). An enhancement in the oxidation current of the chitosan-GD electrode was due to the synergistic effect of effective oxidation ability and an

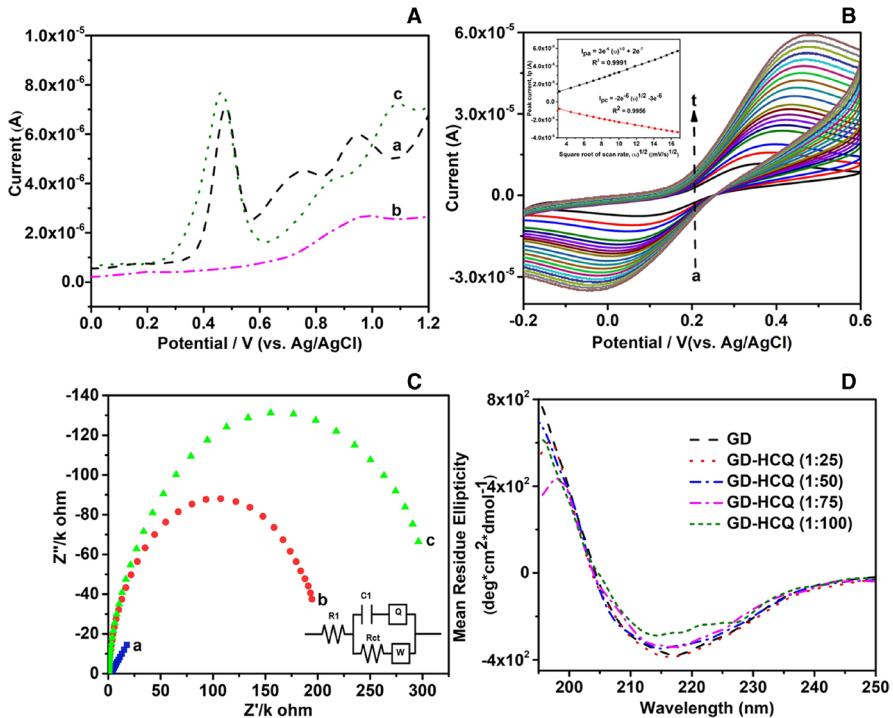


**Fig. 3** A Differential pulse voltammetry of (a) GCE, (b) chitosan/GCE, and (c) chitosan-GD recorded in the presence of 1  $\mu\text{M}$  HCQ and 5  $\mu\text{M}$  ferrocene in  $\text{N}_2$ -saturated 0.01 M phosphate-buffered saline pH 7.4 at a scan rate of 10 mV/s. B Cyclic voltammetry curves of chitosan-GD against various scan rates of (10 to 300 mV/s) in 5 mM  $\text{Fe}(\text{CN})_6^{3-/4-}$  containing 0.1 M KCl; relationship between peak current versus square root of scan rate for GFP Dopa on chitosan/GCE. C Electrochemical impedance spectra (EIS) were recorded in 5 mM  $\text{Fe}(\text{CN})_6^{3-/4-}$  containing 0.1 M KCl as supporting electrolyte on modified GCE surfaces: (a) GCE, (b) chitosan, and c chitosan-GD using frequency range from 0.01 Hz to 10 kHz at potential 0.2 V. D Secondary structure of GD (4  $\mu\text{M}$ ) with various concentrations of HCQ treated samples (25–100  $\mu\text{M}$ )

increase in electrochemically active surface area which further helps to interact the bio-redox protein with HCQ. In addition, this bio-redox protein helps in the transfer of electrons, a stable probe with enhanced electrocatalytic property for the oxidation of HCQ. The combined effect of electrode fabrication by chitosan and GD resulted in enhance in oxidation current. This may be due to the pH-dependent monolayer deposition on the electrode surface by chitosan through an anodic current and the genetically encoded bio-redox protein also gets deposited on the chitosan/GCE. Hence, it is notable that chitosan-GD plays an important role in the synergistic enhancement of the catalytic activities of bio-redox protein as well as providing a matrix for more loading of HCQ.

### Effect of Electrochemical Evaluation of Bio-redox Capacitor Stability

The electrochemical performances of the modified chitosan-GD as a stable electrode material was evaluated through CV using a standard solution of 5 mM Fe (CN)<sub>6</sub><sup>3-/4-</sup> redox probe in 0.01 M PBS pH 7.4. Figure 3B displays the CV curves of the chitosan-GD modified electrode at a scan rate of 10 to 300 mV/s which indicates a subsequent increase in redox peak currents (Ip) of anodic (Ipa) and cathodic (Ipc) peak currents. The peak current ratio of anodic and cathodic was found to be 0.999 at 300 mV/s which indicates that the redox quasi-reversible of chitosan-GD/GCE electrode was good. Simultaneously, because of the increase in peak difference, potential values increase with the scan rate of both the positive shift of anodic peak current and negative shift of cathodic peak current. Therefore, it proves that a quasi-reversible process takes place at the electrode surface.

The electron transfer properties and interfacial properties of the fabricated electrode surface at each deposition process were analyzed using EIS in 5 mM Fe (CN)<sub>6</sub><sup>3-/4-</sup> solution. The Nyquist plot of impedance spectra is shown in Fig. 3C, and the values of charge transfer resistance (Rct) are directly proportional to the diameter of the semicircles. The Rct values of GCE, chitosan, and chitosan-GD were found to be 2.3, 198, and 298 kΩ, respectively. When the chitosan was modified onto the bare GCE, the diameter of the impedance semicircle curve enlarged and the Rct of chitosan/GCE increased concerning GCE. The reason for this may be the chitosan probe formed some interface resistance which restricts the transfer of electrons on the electrode surface. Furthermore, when bio-redox protein was deposited on the chitosan-modified electrode, the diameter of the semicircle significantly increases which indicates that the Rct value gets increased due to the bound bio-redox protein with its non-electroactive properties obstructing electron transfer. Hence, it suggests that enhanced surface area leads to an increase in the electrode sensitivity toward the HCQ.

### Secondary Structural Interaction of the Bio-redox Protein with HCQ

To decipher, the secondary structural changes induced by HCQ, the circular dichroism (CD) spectra of GD with varying concentrations of HCQ were measured. Naturally, GFP has a unique β-can structure built with 11 β-pleated sheets; therefore, a characteristic strong negative band around 215–216 nm was observed for GD during CD spectroscopic analysis. The β-can structure remains similar in the presence of HCQ, except at higher concentrations where a slight decrease in intensity was

noticed. Nevertheless, the overall dichroic profile of GD confirmed that the secondary structure of protein did not get affected significantly after the treatment with varying molar ratios of HCQ (Fig. 3D). From the quantitative CD data analysis, we could observe that the percentage of  $\beta$ -sheet decreases slightly when the concentration of HCQ increases (Table 1) which is consistent with the CD spectra.

### Interaction of HCQ with Bio-redox Protein in Terms of Solution

To understand the interaction of HCQ with GD, the fluorescence spectra of the chromophore along with the various concentrations (0 to 210  $\mu\text{g/ml}$ ) of HCQ were measured. HCQ concentration of 210  $\mu\text{g/ml}$  leads to 80% fluorescence quenching with GD (Fig. 4A). Meanwhile, more than 50% fluorescent intensity of native GFP remained in the presence of 210  $\mu\text{g/ml}$  of HCQ (Fig. 4B). The binding of HCQ with GD did not show any spectral shift in its fluorescent excitation and emission maximum. A calibration curve was generated for GD by plotting the amount of fluorescence quenching against HCQ concentration (Fig. 4C). To understand the specificity of the GD with HCQ, cross-reactivity was carried out with surrogates of drugs (210  $\mu\text{g/ml}$  concentration of mefloquine, primaquine, chloroquine, and HCQ); among them, HCQ showed the highest amount of fluorescence quenching (Fig. 4D).

$$\Delta F/\Delta F_{\max} = (K^d + [\text{HCQ}] + [\text{P}] \pm \sqrt{(K^d + [\text{HCQ}] + [\text{P}])^2 - 4[\text{HCQ}][\text{P}]})/2[\text{P}]$$

where  $\Delta F$  is the change in measured fluorescence,  $\Delta F_{\max}$  is the maximum fluorescence change,  $[\text{P}]$  is the total protein concentration,  $K_d$  is the dissociation constant of the drug binding site, and  $[\text{HCQ}]$  is the total concentration of a drug. The dissociation constant of GD was identified as  $0.65 \pm 0.03 \mu\text{M}$  which indicates the high affinity toward the HCQ. It suggests that the HCQ interaction with GD is static and results in increasing the concentration of HCQ to reduce the chromophore fluorescence.

### Binding of HCQ with Bio-redox Protein

To ascertain the HCQ interaction with GD, we have performed the saturation transfer difference nuclear magnetic resonance (STD NMR) experiment on the GD-HCQ complex. The STD NMR allows differentiating binding ligands from non-binding ligands by selectively saturating protein magnetization and quickly transferring them from protein to the ligands [39–42]. In such a situation, STD NMR produces signals only for the ligands which are spatial proximity (binding) to the protein while the response

**Table 1** Percentage of the secondary structure of GD and GD-HCQ samples, as calculated from CD spectra

Sl. no	Samples	$\alpha$ -Helix (%)	$\beta$ -Sheet (%)	$\beta$ -Turns (%)	Extended chains (%)
1	GD	3.83	51.5	16.1	28.77
2	GD-HCQ (1:25)	3.64	50.9	22.35	23.11
3	GD-HCQ (1:50)	3.49	49.8	24.6	21.96
4	GD-HCQ (1:75)	3.35	47.82	27.6	21.7
5	GD-HCQ (1:100)	3.2	45.05	25.3	26.45

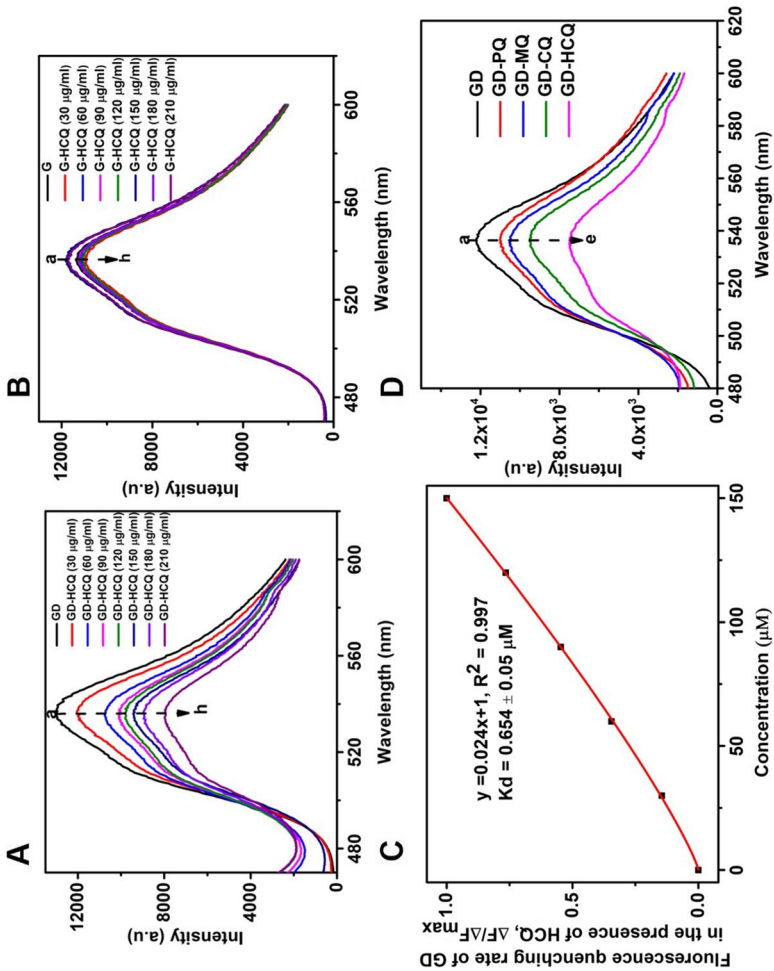


**Fig. 4** **A** and **B** Fluorescence spectrum of GD and G (GFP) at 3  $\mu M$  in the presence of various HCQ concentrations from 0 to 210  $\mu g/ml$  (a to h), **C** fluorescence quenching rate of GD in the presence of HCQ and **D** interference of GD in the presence of various quinine-based drugs (a to e; PQ, primaquine (210  $\mu g/ml$ ); MQ, mefloquine (210  $\mu g/ml$ ); CQ, chloroquine (210  $\mu g/ml$ ); and HCCQ, hydroxychloroquine (210  $\mu g/ml$ ))

from the non-binding ligands is absent. Besides, the site-specific interaction of ligand (receptor) molecules can be obtained by following the epitope mapping of ligand protons. Therefore, herein, the spatial proximity of the HCQ molecule concerning GFP and GD was determined. Furthermore, the interaction sites of HCQ were visualized by creating epitope maps (Fig. 5A and B). Figure 5A (i) shows the proton NMR spectra of HCQ in the absence and presence of saturation transfer (STD). Although the proton signals of HCQ are weak in the STD NMR spectrum (bottom), the existence of signals confirms that HCQ molecules are in proximity to the protein (Fig. 5A (ii)). In the absence of saturation, all the protons of HCQ need to be accounted but only a few protons have appeared in the STD-NMR which suggests that the observed protons are close to the protein compared to other protons in the HCQ molecule. Furthermore, the difference in the proton epitope mapping of HCQ between G-HCQ and GD-HCQ (Fig. 5A and B, Table 2) suggests that interaction sites of HCQ with GFP could be different from GD (Fig. 5A (i) and B (i)). Considering the STD signals, the closest interaction sites of HCQ with GFP and GD could be the aliphatic region, especially methyl and methylene groups of the HCQ molecule. The STD-NMR analyses thus evidently support that HCQ molecules are in proximity to both GFP and GD proteins and the mode of interaction through the alkyl part of HCQ.

### Three-Dimensional Determination of HCQ Binding with Bio-redox Protein

To further determine the possible HCQ interaction with GD, we generated a three-dimensional model structure of the GFP variant through homology modeling. Based on the energy minimized model, we surmise that the three residues LYS161, ASP155, GLN183, and flexible loop regions are closely interacting with HCQ. The alkyl part of the HCQ is closer to the LYS161 side chain in S1 and S2 sites (Fig. 5C (i) and (ii)) and showed a similar interaction pattern with other places. The replacement of DOPA in the protein ameliorates the HCQ to the proximity that could facilitate the electron transfer during the redox cycle. The structural analysis supports the STD-NMR data and confirmed that the genetic incorporation of DOPA favor proximity HCQ for interaction with protein through the alkyl part of molecules.

### Electrochemical Detection of Hydroxychloroquine

The sensitivity of chitosan-GD towards HCQ was analyzed through DPV (Fig. 6A). The oxidation current shows the recorded DPV with the utilization of 0.01 M PBS at pH 7.4 for chitosan-GD/GCE, and the corresponding linearity plot exhibited after the addition of HCQ, where the limit of detection (LOD) of the sensor can be assessed from the standard calculation ( $\text{LOD} = 3\sigma/m$ ), whereas  $\sigma$  represents the standard deviation of the replicates of sensor blank experiments and  $m$  is the slope of the calibration plot. Figure 6A shows the stable and reproducible DPV voltammograms of HCQ with various concentrations from 92 nM to 4.4  $\mu\text{M}$ . With the continuous addition of HCQ in the electrochemical cell, the result shows a steady-state rise in the oxidation current of HCQ at 1.08 V. Similarly, the HCQ calibration plot signifies the sensitivity and the voltammetric analysis of HCQ at the

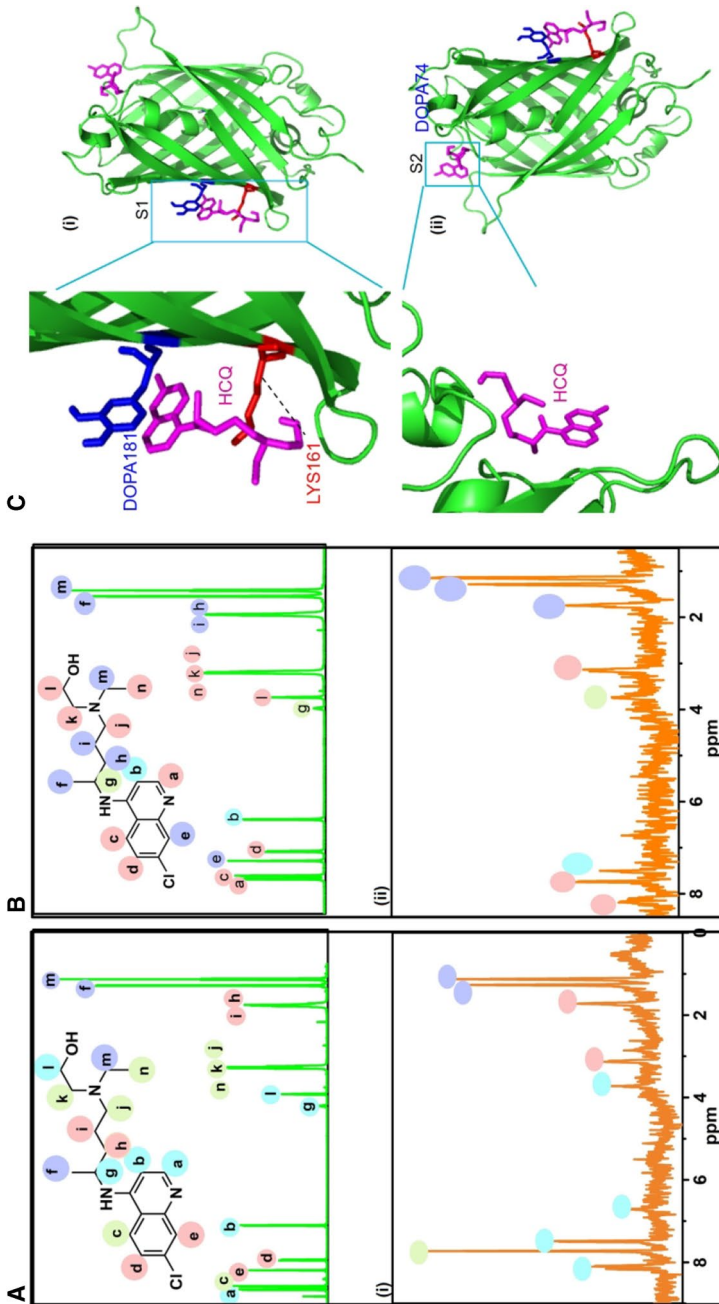


**Fig. 5** **A** <sup>1</sup>H NMR spectrum (green) and the corresponding (i) STD-NMR of G (orange) in the presence of HCQ (50 mM). **B** <sup>1</sup>H NMR spectrum (green) and the corresponding (i) STD NMR (orange) of GD in the presence of HCQ (50 mM). The concentration of the G and GD were 5  $\mu$ M. **C** Three-dimensional modal structure of GFP variant interacting with HCQ through homology modeling (i) S1 site and (ii) S2 site of GD

**Table 2** Percentage of G and GD-HCQ samples, as calculated from STD-NMR

Samples	STD-NMR (%)			
	0–25	25–50	50–75	75–100
G-HCQ	a, b, g, l	c, n, k, j	i, h, e, d	f, m
GD-HCQ	b	g	n, k, j, l, d, a, c	m, f, i, h, e

chitosan-GD-fabricated electrode exhibited a signal to noise factor of 3 ( $S/N = 3$ ) and LOD value was found to be 58 nM (Fig. 6B). Therefore, when compared with already reported approaches for the detection of HCQ, the developed bio-redox-based sensor exhibited superiority, sensitivity, selectivity, and less analytical time (Table 3).

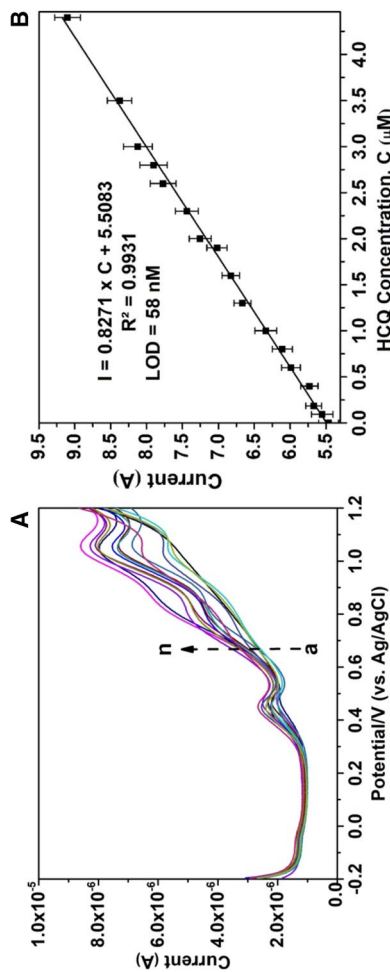


**Fig. 6** A Detection of HCQ by chitosan-GD electrode using differential pulse voltammetry obtained at a scan rate of 10 mV/s in 0.01 M PBS (pH 7.4) containing (a to p, 4.4 μM to 92 nM and 5 μM ferrocene). B A calibration curve (peak current vs HCQ concentration) for chitosan-GD electrode. Error bar, SD;  $n = 3$



**Table 3** Comparison of different sensors for HCQ detection

Sl. no	Method	Linear range	Detection Limit	References
1	DPV	$2 \times 10^{-5}$ – $5 \times 10^{-4}$ M	$11.2 \times 10^{-6}$ M	1
2	DPV	$7.4 \times 10^{-8}$ – $11.9 \times 10^{-6}$ M	$4.7 \times 10^{-9}$ M	2
3	DPV	$5.7 \times 10^{-8}$ – $1 \times 10^{-4}$ M	$6 \times 10^{-9}$ M	3
4	SWV	$0.2$ – $9 \times 10^{-6}$ M	$0.06 \times 10^{-6}$ M	4
5	UV–Vis	$8$ – $12 \times 10^{-6}$ M	$0.38 \times 10^{-6}$ M	5
6	UV–Vis	$2$ – $12 \times 10^{-6}$ M	$0.3145 \times 10^{-6}$ M	6
7	HPLC	-	$29.76 \times 10^{-6}$ M	7
8	HPLC	-	$29.76 \times 10^{-9}$ M	8
9	DPV	$9.2 \times 10^{-10}$ – $4.4 \times 10^{-6}$ M	$58 \times 10^{-9}$ M	Present study

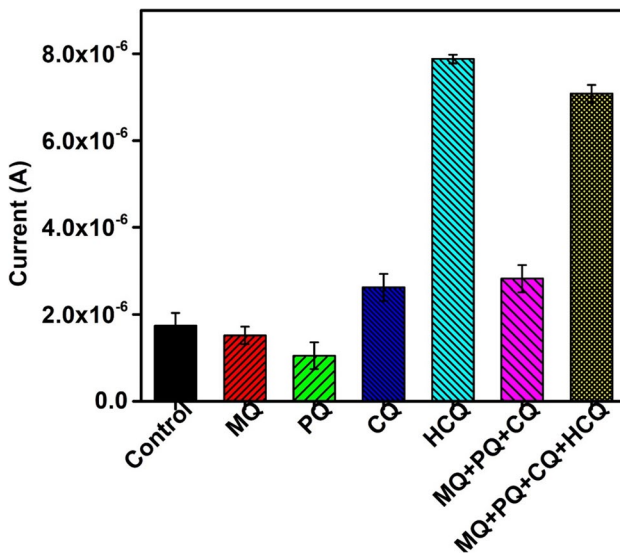


**Fig. 7** Differential pulse voltammetry response on chitosan-GD for control; mefloquine (MQ) (450 nM); primaquine (PQ) (450 nM); chloroquine (CQ) (450 nM), and HCQ (45 nM), a combination of MQ+PQ+CQ in the absence and presence of HCQ in 0.01 M phosphate-buffered saline (pH 7.4) at a scan rate of 50 mV/s with 5  $\mu$ M ferrocene

### Cross-reactivity Studies

The electrochemical sensor was established for the interference of cross-reactivity studies with closely related mefloquine, primaquine, chloroquine, and a combination of all three drugs (MQ, PQ, CQ) in the presence and absence of HCQ, whereas all the drug molecules were in 10 times higher concentration than HCQ. Figure 7 showed that negligible interference was observed for closely related drug molecules. The results confirmed that the designed electrochemical sensor exhibited high specificity

**Table 4** Determination of HCQ in spiked urine samples

Samples	Added ( $\mu\text{M}$ )	Found ( $\mu\text{M}$ ) <sup>[a]</sup>	Recovery (%)
Sample A	1.5	1.47	98.00
	2.0	1.98	99.00
	4.0	4.01	100.3
Sample B	1.5	1.46	97.3
	2.0	1.89	94.5
	4.0	3.89	97.3
Sample C	1.5	1.51	100.7
	2.0	2.02	101.0
	4.0	4.01	100.3

<sup>[a]</sup>Average values calculated from three determinations

for HCQ detection. The reproducibility and stability of the chitosan-GD electrode were also explored by preparing ten distinct electrodes in a similar condition and verified with 45 nM HCQ. The RSD of 2.4% was detected, conforming high reproducibility of the chitosan-GD electrode fabrication. On the other hand, an additional set of ten chitosan-GD electrodes were stored at ambient temperature for four weeks, which showed a relative standard deviation of 2.8%.

### HCQ Evaluation in Spiked Urine Samples

The performance and reliability of the developed genetically encoded bio-redox protein towards HCQ sensing were assessed in real urine samples and were spiked with various concentrations of HCQ and diluted to 10 ml with 0.01 mM PBS at pH 7.4. The recovery values for HCQ in samples A, B, and C exhibited > 98%, and the results are summarized in Table 4 and Fig. 8. From the results, it may be concluded that the developed bio-redox protein-based sensor could be a systematic benchmark for quality control analysis of the drugs in medicinal and biological applications.

### Conclusions

We have developed a genetically encoded bio-redox responsive molecular sensor by anodic deposition of redox protein on the chitosan-modified electrode which is a promising platform for ultrasensitive detection of HCQ. We postulated that the developed bio-redox capacitor exhibits enhanced electrochemically active surface area which could indirectly enhance the specificity and selectivity of HCQ. The fabricated bio-redox capacitor encoded catechol moieties grafted on the chitosan establishes communication and transfer of electrons between the electrode for sensing HCQ. Notably, the developed bio-redox capacitor exhibited an excellent detection limit of 58 nM. Interestingly, it is reusable, durable, and reproducible and exhibits electron shuttling, allowing transmission of HCQ as a spatiotemporal redox command. We anticipate that the genetically encoded bio-capacitor-based sensors will enable the

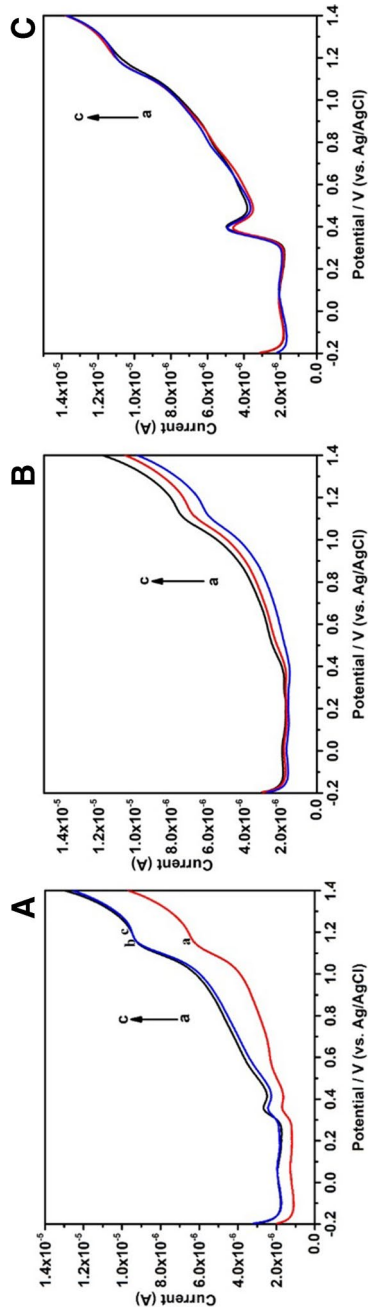


**Fig. 8** Differential pulse voltammograms of bio-redox protein-based sensor for the monitoring of HCQ in three different spiked urine samples of **A**, **B**, and **C** (with 1.5  $\mu\text{M}$  (a), 2.0  $\mu\text{M}$  (b), and 4.0  $\mu\text{M}$  (c))

development and design of custom-made bioelectronics devices that could transform biological function as well as detect target specific molecules for medical and environmental applications. To the best of our knowledge, this is the first demonstration of coupling NCAA incorporation with bioelectronics for drug screening and protein assembly appropriate for industrial, biomedical, and environmental domains.

**Acknowledgements** The first author Mrs. Asuma Janeena thankfully acknowledges the University Grant Commission (UGC), India, for the award of UGC-SRF throughout the research. SE and NJ thank DST for the financial support under Water IC for SUTRAM of EASY WATER (DST/TM/WTI/WIC/2K17/82(C)). The authors gratefully acknowledge the Council of Scientific and Industrial Research (CSIR), New Delhi, for funding this research through Focused Basic Research (FBR) MLP-2006.

**Author Contribution** Asuma Janeena: Development of genetically modified protein, experimental analysis, and manuscript writing. Narayanan J: Electrochemical method and analysis. Ganesh Shanmugam: STD-NMR and CD analysis. Easwaramoorthi Shanmugam: XPS and AFM analysis and manuscript correction. Niraikulam Ayyadurai: Innovation, manuscript writing, correction, and supervision.

**Funding** This research was supported by the Indian Council of Medical Research (ICMR), New Delhi, India (ICMR 5/3/8/4/2019-ITR).

## Declarations

**Competing Interests** The authors declare no competing interests.

## References

- Ackerman, N. R., Jubb, S. N., & Marlowe, S. L. (1981). Effects of various anti-inflammatory and anti-rheumatic agents on the synthesis, secretion, and activity of a cartilage proteoglycan-degrading enzyme and other macrophage enzymes. *Biochemical Pharmacology*, *30*, 2147–2155.
- Al-Bari, M. A. A. (2017). Targeting endosomal acidification by chloroquine analogs as a promising strategy for the treatment of emerging viral diseases. *Pharmacology Reserch Perspective*, *5*, e00293.
- Riva, L., Yuan, S., Yin, X., Martin-Sancho, L., Matsunaga, N., Pache, L., Burgstaller-Muehlbacher, S., De Jesus, P. D., Teriete, P., Hull, M. V., Chang, M. W., Chan, J.F.-W., Cao, J., Poon, V.K.-M., Herbert, K. M., Cheng, K., Nguyen, T.-T.H., Rubanov, A., Pu, Y., ... Chanda, S. K. (2020). Discovery of SARS-CoV-2 antiviral drugs through large-scale compound repurposing. *Nature*, *586*, 113–119.
- Singh, A. K., Singh, A., Shaikh, A., Singh, R., & Misra, A. (2020). Chloroquine and hydroxychloroquine in the treatment of COVID-19 with or without diabetes: A systematic search and a narrative review with a special reference to India and other developing countries. *Diabetes and Metabolic Syndrome: Clinical Research and Reviews*, *14*, 241–246.
- Shannon, A., Le, N.T.-T., Selisko, B., Eydoux, C., Alvarez, K., Guillemot, J.-C., Decroly, E., Peersen, O., & Ferron, F. (2020). B Canard Remdesivir and SARS-CoV-2: Structural requirements at both nsp12 RdRp and nsp14 Exonuclease active-sites. *Antiviral Research*, *178*, 104793.
- Ortolani, C., & Pastorello, E. A. (2020). Hydroxychloroquine and dexamethasone in COVID-19: Who won and who lost? *Clinical Molecular Allergy*, *18*, 17.
- Mauthe, M., Orhon, I., Rocchi, C., Zhou, X., Luhr, M., Hijlkema, K.-J., Coppes, R. P., Engedal, N., Mari, M., & Reggiori, F. (2018). Chloroquine inhibits autophagic flux by decreasing autophagosome-lysosome fusion. *Autophagy*, *14*, 1435–1455.
- Popert, A. J. (1976). Chloroquine: A review., *Rheumatol. Rehabilitation*, *15*, 235–238.
- Laaksonen, A.-L., Koskiahde, V., & Juva, K. (1974). Dosage of antimalarial drugs for children with juvenile rheumatoid arthritis and systemic lupus erythematosus: A clinical study with determination of serum concentrations of chloroquine and hydroxychloroquine. *Scandinavian Journal of Rheumatology*, *3*, 103–108.
- Barnard, D. L., Day, C. W., Bailey, K., Heiner, M., Montgomery, R., Lauridsen, L., Chan, P. K. S., & Sidwell, R. W. (2006). Evaluation of immunomodulators, interferons and known in vitro SARS-coV inhibitors for inhibition of SARS-CoV replication in BALB/c mice. *Antiviral Chemistry & Chemotherapy*, *17*, 275–284.


11. Vincent, M. J., Bergeron, E., Benjannet, S., Erickson, B. R., Rollin, P. E., Ksiazek, T. G., Seidah, N. G., & Nichol, S. T. (2005). Chloroquine is a potent inhibitor of SARS coronavirus infection and spread. *Virology Journal*, 2, 69.
12. Wang, M., Cao, R., Zhang, L., Yang, X., Liu, J., Xu, M., Shi, Z., Hu, Z., Zhong, W., & Xiao, G. (2020). Remdesivir and chloroquine effectively inhibit the recently emerged novel coronavirus (2019-nCoV) in vitro. *Cell Research*, 30, 269–271.
13. Gautret, P., Lagier, J.-C., Parola, P., Hoang, V. T., Meddeb, L., Mailhe, M., Doudier, B., Courjon, J., Giordanengo, V., Vieira, V. E., Tissot-Dupont, H., Honoré, S., Colson, P., Chabrière, E., La Scola, B., Rolain, J.-M., Brouqui, P., & Raoult, D. (2020). Hydroxychloroquine and azithromycin as a treatment of COVID-19: results of an open-label non-randomized clinical trial. *International Journal of Antimicrobial Agents*, 56, 105949.
14. G. Augustine, M. Aarthy, H. Thiagarajan, S. Selvaraj, N.R. Kamini, G. Shanmugam, (2021) N.7Ayyadurai, Self-Assembly and Mechanical Properties of Engineered Protein Based Multifunctional Nanofiber for Accelerated Wound Healing. *Advances in Healthcare Materials*. n/a (n.d.) 2001832.
15. Shyr, Z. A., Gorshkov, K., Chen, C. Z., & Zheng, W. (2020). Drug Discovery Strategies for SARS-CoV-2. *Journal of Pharmacology and Experimental Therapeutics*, 375, 127–138.
16. de Santos, I. A., Grosche, V. R., Bergamini, F. R. G., Sabino-Silva, R., & Jardim, A. C. G. (2020). Antivirals against coronaviruses: Candidate drugs for SARS-CoV-2 Treatment? *Frontiers of Microbiology*, 11, 1818.
17. Cui, W., Yang, K., & Yang, H. (2020). Recent progress in the drug development targeting SARS-CoV-2 main protease as treatment for COVID-19. *Frontiers in Molecular Biosciences*, 7, 398.
18. Alexander, S. P. H., Armstrong, J. F., Davenport, A. P., Davies, J. A., Faccenda, E., Harding, S. D., Levi-Schaffer, F., Maguire, J. J., Pawson, A. J., Southan, C., & Spedding, M. (2020). A rational roadmap for SARS-CoV-2/COVID-19 pharmacotherapeutic research and development: IUPHAR Review 29. *British Journal of Pharmacology*, 177, 4942–4966.
19. Ilamaran, M., Janeena, A., Valappil, S., Ramudu, K. N., Shanmugam, G., & Niraikulam, A. (2019). A self-assembly and higher order structure forming triple helical protein as a novel biomaterial for cell proliferation. *Biomaterials Science*, 7, 2191–2199.
20. Pandey, A., Nikam, A. N., Shreya, A. B., Mutalik, S. P., Gopalan, D., Kulkarni, S., Padya, B. S., Fernandes, G., Mutalik, S., & Prassl, R. (2020). Potential therapeutic targets for combating SARS-CoV-2: Drug repurposing, clinical trials and recent advancements. *Life Sciences*, 256, 117883.
21. Y. Orooji, H. Sohrabi, N. Hemmat, F. Oroojalian, B. Baradaran, A. Mokhtarzadeh, M. Mohaghegh, H. Karimi-Maleh, (2021) An overview on SARS-CoV-2 (COVID-19) and other human coronaviruses and their detection capability via amplification assay, Chemical Sensing, Biosensing, Immunosensing, and Clinical Assays. *Nano-Micro Letters* 13, 18.
22. Dixon, T. A., Williams, T. C., & Pretorius, I. S. (2021). Sensing the future of bio-informational engineering. *Nature Communications*, 12, 388.
23. Muskovich, M., & Bettinger, C. J. (2012). Biomaterials-based electronics: Polymers and interfaces for biology and medicine. *Advances in Healthcare Materials*, 1, 248–266.
24. Asuma Janeena, J., Ilamaaran, M., George, A., George Sebastian, A., Sreeram Raghavan, S., & Suryalakshmi, L. (2018). P, Aarthy M, Kamini N R, Gunasekharan K, Ayyadurai N, Biomimetic strategies to design metallic proteins for detoxification of hazardous heavy metal. *Journal of Hazardous Materials*, 358, 92–100.
25. Kim, E., Liu, Z., Liu, Y., Bentley, W. E., & Payne, G. F. (2018). Erratum: Catechol-based hydrogel for chemical information processing. *Biomimetics*, 2, 3–11.
26. Wu, S., Kim, E., Li, J., Bentley, W. E., Shi, X.-W., & Payne, G. F. (2019). Catechol-based capacitor for redox-linked bioelectronics. *ACS Applied Electronic Materials*, 1, 1337–1347.
27. VanArsdale, E., Pitzer, J., Payne, G. F., & Bentley, W. E. (2020). Redox electrochemistry to interrogate and control biomolecular communication. *IScience*, 23, 101545.
28. Janeena, A., Prem, S., Mohandass, P., Ashokraj, S., Narayanan, J., Easwaramoorthi, S., & Ayyadurai, N. (2022). Selection and screening of genetically encoded fluorescent protein as a sensor for cancer theranostics. *Biosensors Bioelectronics X*, 10, 100129.
29. Hwang, D.-W., Lee, S., Seo, M., & Chung, T. D. (2018). Recent advances in electrochemical non-enzymatic glucose sensors – A review. *Analytica Chimica Acta*, 1033, 1–34.
30. Koskun, Y., Şavk, A., Şen, B., & Şen, F. (2018). Highly sensitive glucose sensor based on monodisperse palladium nickel/activated carbon nanocomposites. *Analytica Chimica Acta*, 1010, 37–43.
31. Chen, S., Yu, Y.-L., & Wang, J.-H. (2018). Inner filter effect-based fluorescent sensing systems: A review. *Analytica Chimica Acta*, 999, 13–26.
32. Ilamaran, M., Sundarapandian, A., Aarthy, M., Shanmugam, G., Ponesakki, G., Ramudu, K. N., & Niraikulam, A. (2020). Growth factor-mimicking 3{,}4-dihydroxyphenylalanine-encoded bioartificial

- extracellular matrix like protein promotes wound closure and angiogenesis. *Biomaterials Science*, 8, 6773–6785.
33. Li, F., Yu, Z., Han, X., & Lai, R. Y. (2019). Electrochemical aptamer-based sensors for food and water analysis: A review. *Analytica Chimica Acta*, 1051, 1–23.
  34. Ayyadurai, N., Prabhu, N. S., Deepankumar, K., Jang, Y. J., Chitrapriya, N., Song, E., et al. (2011). Bioconjugation of 1-3,4-dihydroxyphenylalanine containing protein with a polysaccharide. *Bioconjugate Chemistry*, 22, 551–555.
  35. Kim, E., Leverage, W. T., Liu, Y., White, I. M., Bentley, W. E., & Payne, G. F. (2014). Redox-capacitor to connect electrochemistry to redox-biology. *The Analyst*, 139, 32–43.
  36. Yi, H., Wu, L.-Q., Bentley, W. E., Ghodssi, R., Rubloff, G. W., Culver, J. N., & Payne, G. F. (2005). Biofabrication with Chitosan. *Biomacromolecules*, 6, 2881–2894.
  37. Aarthy, M., George, A., & Ayyadurai, N. (2021). Beyond protein tagging: Rewiring the genetic code of fluorescent proteins – A review. *International Journal of Biological Macromolecules*, 191, 840–851.
  38. Eschbach, S., Hofmann, C., Maerz M., Maier, U-G., Sitte, P. (1990). Molecular Cloning. A Laboratory Manual. 2. Auflage. Hrsg. von J. Sambrook, E. F. Fritsch, T. Maniatis, Cold Spring Harbor Laboratory Press, Cold Spring Harbour 1989, 115. *Biologie in Unserer Zeit*, 20, 285.
  39. Ilamaran, M., Sriram Raghavan, S., Karthik, S., Sanjay Nalawade, K., Samvedna, S., Routray, W., Kamini, N. R., Saravanan, P., & Ayyadurai, N. (2019). A facile method for high level dual expression of recombinant and congener protein in a single expression system. *Protein Expression and Purification*, 156, 1–7.
  40. Lampel, A., McPhee, S. A., Park, H.-A., Scott, G. G., Humagain, S., Hekstra, D. R., Yoo, B., Frederix, P. W. J. M., Li, T.-D., Abzalimov, R. R., Greenbaum, S. G., Tuttle, T., Hu, C., Bettinger, C. J., & Ulijn, R. V. (2017). Polymeric peptide pigments with sequence-encoded properties. *Science*, 356, 1064–1068.
  41. Mayer, M., & Meyer, B. (2001). Group epitope mapping by saturation transfer difference NMR to identify segments of a ligand in direct contact with a protein receptor. *Journal of the American Chemical Society*, 123, 6108–6117.
  42. Dalvit, C., Fagerness, P. E., Hadden, D. T. A., Sarver, R. W., & Stockman, B. J. (2003). Fluorine-NMR experiments for high-throughput screening: Theoretical aspects, practical considerations, and range of applicability. *Journal of the American Chemical Society*, 125, 7696–7703.

**Publisher's Note** Springer Nature remains neutral with regard to jurisdictional claims in published maps and institutional affiliations.

Springer Nature or its licensor holds exclusive rights to this article under a publishing agreement with the author(s) or other rightsholder(s); author self-archiving of the accepted manuscript version of this article is solely governed by the terms of such publishing agreement and applicable law.

## Authors and Affiliations

Asuma Janeena<sup>1,2</sup> · Narayanan Jayaraman<sup>3</sup> · Ganesh Shanmugam<sup>2,4</sup> · Shanmugam Easwaramoorthi<sup>2,3</sup> · Niraikulam Ayyadurai<sup>1,2</sup> 

<sup>1</sup> Biotechnology and Biochemistry, Council of Scientific and Industrial Research (CSIR)-Central Leather Research Institute, Chennai, India

<sup>2</sup> Academy of Scientific and Industrial Research (AcSIR), 201002, Ghaziabad, India

<sup>3</sup> Inorganic and Physical Chemistry, Council of Scientific and Industrial Research (CSIR)-Central Leather Research Institute, Chennai, India

<sup>4</sup> Organic and Bio-Organic Chemistry, Council of Scientific and Industrial Research (CSIR)-Central Leather Research Institute, Chennai, India